The Astrophysical Journal, 906:44 (7pp), 2021 January 1 https://doi.org/10.3847/1538-4357/abc703

Silicon and Hydrogen Chemistry under Laboratory Conditions Mimicking the Atmosphere of Evolved Stars

Mario Accolla[1], Gonzalo Santoro[1], Pablo Merino[1,2], Lidia Martínez[1], Guillermo Tajuelo-Castilla[1], Luis Vázquez[1], Jesús M. Sobrado[3], Marcelino Agúndez[2], Miguel Jiménez-Redondo[4], Víctor J. Herrero[4], Isabel Tanarro[4], José Cernicharo[2], and José Ángel Martín-Gago[1]

[1] Instituto de Ciencia de Materiales de Madrid (ICMM, CSIC), Materials Science Factory, Group of Interdisciplinary Studies based on Nanoscopic Systems, c/ Sor Juana Inés de la Cruz 3, E-28049 Cantoblanco, Madrid, Spain; mario.accolla@csic.es, gonzalo.santoro@icmm.csic.es, gago@icmm.csic.es
[2] Instituto de Física Fundamental (IFF, CSIC), Group of Molecular Astrophysics, c/ Serrano 123, E-28006 Madrid, Spain
[3] Centro de Astrobiología (CAB, INTA-CSIC), Crta. de Torrejón a Ajalvir km 4, E-28850, Torrejón de Ardoz, Madrid, Spain
[4] Instituto de Estructura de la Materia (IEM, CSIC), Molecular Physics Department, c/ Serrano 123, E-28006 Madrid, Spain
Received 2020 June 26; revised 2020 October 27; accepted 2020 November 1; published 2021 January 5

Abstract

Silicon is present in interstellar dust grains, meteorites and asteroids, and to date 13 silicon-bearing molecules have been detected in the gas phase toward late-type stars or molecular clouds, including silane and silane derivatives. In this work, we have experimentally studied the interaction between atomic silicon and hydrogen under physical conditions mimicking those in the atmosphere of evolved stars. We have found that the chemistry of Si, H, and H_2 efficiently produces silane (SiH_4), disilane (Si_2H_6) and amorphous hydrogenated silicon (a-Si:H) grains. Silane has been definitely detected toward the carbon-rich star IRC +10216, while disilane has not been detected in space yet. Thus, based on our results, we propose that gas-phase reactions of atomic Si with H and H_2 are a plausible source of silane in C-rich asymptotic giant branch stars, although its contribution to the total SiH_4 abundance may be low in comparison with the suggested formation route by catalytic reactions on the surface of dust grains. In addition, the produced a-Si:H dust analogs decompose into SiH_4 and Si_2H_6 at temperatures above 500 K, suggesting an additional mechanism of formation of these species in envelopes around evolved stars. We have also found that the exposure of these dust analogs to water vapor leads to the incorporation of oxygen into Si–O–Si and Si–OH groups at the expense of SiH moieties, which implies that if this kind of grain is present in the interstellar medium, it will probably be processed into silicates through the interaction with water ices covering the surface of dust grains.

Unified Astronomy Thesaurus concepts: Interstellar dust (836); Interstellar dust processes (838); Silicate grains (1456); Laboratory astrophysics (2004); Astrochemistry (75)

1. Introduction

Hydrogen and helium constitute more than 99% of the matter in the universe. Among the trace elements, silicon is the fifth most abundant, being a usual component of the solid refractory material spread in interstellar and circumstellar clouds. Silicon has been identified in the dust grains formed around evolved stars through infrared emission bands, in the form of solid SiC in carbon-rich sources (Treffers & Cohen 1974) and silicates, both amorphous and crystalline, around oxygen-rich stars (Waters et al. 1996; Henning 2010). Silicates are also a major constituent of interstellar dust grains (Fogerty et al. 2016). To date, 13 silicon-bearing molecules have been detected in the gas phase toward the carbon-rich star IRC +10216 and in a few other sources. SiO and SiS were the first species detected toward evolved stars and molecular clouds by comparison with their laboratory spectra (Törring 1968; Tiemann et al. 1972). Among the other silicon-bearing species, SiC (Cernicharo et al. 1989), SiC_2 (Thaddeus et al. 1984), and Si_2C (Cernicharo et al. 2015) are the most promising candidates as seeds of SiC dust in carbon-rich stars (Massalkhi et al. 2018). Other silicon-bearing species found in the envelopes of carbon-rich evolved stars are SiN (Turner 1992), SiH_3CN (Agúndez et al. 2014; Cernicharo et al. 2017), SiH_3CH_3 (Cernicharo et al. 2017), SiC_3 (Apponi et al. 1999), SiC_4 (Ohishi et al. 1989), SiCN (Guélin et al. 2000), and SiNC (Guélin et al. 2004). Silane (SiH_4) has been observed through the rovibrational transitions near 917 cm^{-1} (Goldhaber & Betz 1984; Keady & Ridgway 1993) toward the carbon-rich star IRC +10216.

To investigate the formation of silicon-containing species in astrophysical environments, most of the laboratory experiments employed SiH_4 as the molecular precursor. For instance, mixtures of silane and CO or C_2H_2 subjected to low pressure discharges efficiently produce SiO, SiC, SiC_2 and other SiC_n molecules, already detected in space (McCarthy et al. 2003). Moreover, as discussed by Kaiser & Osamura (2005), several authors studied the photochemistry of SiH_4 and the subsequent production of hydrogenated silicon clusters, such as SiH_2 and SiH, thus suggesting a rich silane chemistry occurring in circumstellar envelopes (CSEs). In fact, these radicals can react with the surrounding species (for instance CH_4) to form organosilicon molecules. Recently, the interaction of the silyldyne (SiH) radical and excited atomic Si with hydrocarbons have also been shown to lead to the formation of complex organosilicon molecules such as those ubiquitously found in the CSE of IRC+10216 (Yang et al. 2015, 2019).

Since the 1970s, the solar cell industry has encouraged the study of the thermal decomposition and nucleation of silane, which is one of the methods to produce solar-grade silicon with applications for solar cells. For instance, Wyller et al. (2016) studied the particle nucleation from the decomposition of SiH_4 in a H_2 atmosphere as a function of temperature in a free-space reactor. The formation of SiH_4 itself from its simplest components, i.e., Si and H_2, has been experimentally investigated by Hanfland et al. (2011) by compressing

(124 GPa) elemental silicon and hydrogen at room temperature into a diamond anvil cell, i.e., at conditions far removed from those in the CSEs of asymptotic giant branch (AGB) stars.

In this work, we investigate the chemistry of atomic silicon and hydrogen, under conditions mimicking those reported for the circumstellar regions of AGB stars, using the Stardust machine, an experimental station allowing for the synthesis, processing and in situ characterization of the gaseous products and dust analogs produced from atomic precursors (Martínez et al. 2020; Santoro et al. 2020a). We show that the interaction between Si atoms, H, and H_2 efficiently generates silane (SiH_4), disilane (Si_2H_6), and amorphous hydrogenated silicon (a-Si:H) grains. Furthermore, we show that the thermal decomposition of the a-Si:H dust analogs produces SiH_4 and Si_2H_6 as well. The a-Si:H analogs also exhibit a high reactivity when exposed to water vapor, incorporating oxygen into Si–O and Si–OH moieties. We discuss the implications of our experimental results for the chemistry occurring in CSEs around AGB stars.

2. Experiments

The synthesis and characterization of the products of the $Si + H_2$ reaction have been performed with the Stardust machine, which has been thoroughly described elsewhere (Martínez et al. 2018, 2020; Santoro et al. 2020a, 2020b). Briefly, this experimental station is based on the use of a sputtering gas aggregation source (SGAS) to extract atoms from a solid target by means of magnetron sputtering. Inside the aggregation zone of the SGAS, the atoms condense into molecules and nanoparticles. In addition, it is possible to inject gases inside the aggregation zone to promote gas-phase chemical reactions during nanoparticle formation. A battery of in situ diagnostic techniques is available for characterizing both the gas-phase and solid-phase products. Moreover, a fast entry port allows the collection of solid samples for ex situ analysis. The complete system is kept at an ultrahigh vacuum (UHV) with a base pressure of 2×10^{-10} mbar, ensuring an ultraclean environment for both the synthesis and characterization of the analogs.

In the present study, a polycrystalline silicon target (99.99% purity) was used to vaporize silicon atoms by radiofrequency magnetron sputtering, using argon as the sputtering gas with a flow rate of 150 sccm. The power applied to the magnetron was 100 W. A controlled flow of H_2 (99.99% purity) was injected into the aggregation zone at flow rates of 0, 0.15, 1, and 5 sccm. The solid dust analogs analyzed were produced using a flow rate of 1 sccm.

Optical emission spectroscopy (OES) of the sputtering plasma was performed inside the aggregation zone at a distance of around 1 cm from the magnetron target through a fused silica window. A Czerny–Turner spectrograph (Shamrock SR-193-i-A, Andor) with a CCD camera (iDus DU420A-BVF) was employed with a spectral resolution of 0.15 nm.

Mass spectrometry was carried out with a Pfeiffer HiQuad QMG 700 with QMA 400 mass spectrometer (mass range of 0–512 amu) and a CP 400 ion counter preamplifier.

Morphological characterization of the dust analogs was performed ex situ by atomic force microscopy (AFM). The dust analogs were collected on SiO_x substrates, and a Nanoscope IIIA (Veeco) AFM System was employed. All images were analyzed using the WSxM software (Horcas et al. 2007).

Fourier transform infrared (FTIR) spectroscopy was performed in situ in transmission geometry. The dust analogs were deposited on KBr substrates and transferred to a separated UHV chamber (Santoro et al. 2020b) using a UHV suitcase ($P < 5 \times 10^{-9}$ mbar). A Vertex 70 V (Bruker) instrument equipped with a liquid-nitrogen-cooled mercury cadmium telluride detector was employed. The spectral resolution was 2 cm^{-1} and 256 scans were coadded for each spectrum.

Thermal programmed desorption (TPD) experiments were carried out by heating the solid samples up to 650 K with a rate of 10 K $minute^{-1}$ and using the above-mentioned mass spectrometer to detect the desorbing species. For the TPD measurements the dust analogs were collected on a clean Ag (111) substrate.

Finally, X-ray photoelectron spectroscopy (XPS) of the dust analogs was performed in situ using a Phoibos 100 1D electron/ion analyzer with a one-dimensional delay line detector. Freshly cleaved highly ordered pyrolytic graphite was used as substrate.

3. Results

When no H_2 is injected into the system, the presence of sputtered silicon atoms in the magnetron plasma is proven by OES through the line at 288.16 nm (Striganov & Sventitskii 1968). Figure 1(a) shows that the signal originated from excited Si atoms is more intense in the absence of hydrogen. Injecting H_2 promotes an efficient chemistry, and the emission from excited Si atoms decreases as the amount of H_2 increases, nearly vanishing at a flow rate of 5 sccm (Figure 1(a)), whereas the emission of atomic hydrogen (Hα) scales up with the H_2 flow rate (Figure 1(b)), indicating that Si atoms are consumed in the reaction with hydrogen. Figure 1(c) shows the detection of SiH (Perrin & Delafosse 1980) at a flow rate of 0.15 sccm, whose emission decreases as we raise the amount of hydrogen, vanishing when the H_2 flow rate reaches 5 sccm. In addition, a faint emission line is observed at 643.10 nm which can be attributed to the presence of SiH_2 (Escribano & Campargue 1998), whose maximum intensity corresponds as well to a H_2 flow rate of 0.15 sccm (Figure 1(d)). An Ar emission line at 643.15 nm overlaps with the emission of SiH_2. However the different behavior of Ar emission and the line at 643.10 nm versus the H_2 flow rate (Figure 1(e)) supports our assignment. The decrease in Ar intensity with the introduction of reactive gases in the aggregation zone of ion cluster sources is a known process and can be ascribed to the consumption of part of the power applied to the magnetron in the dissociation the reactive gas molecules (Martínez et al. 2018). The behavior of SiH and SiH_2 with respect to the H_2 flow rate suggests a critical concentration of H_2 to trigger an active chemistry.

We estimate that around 10% of the injected H_2 reaches the magnetron, therefore being susceptible to dissociating in the plasma, which produces H atoms that are available to react with Si atoms. The bimolecular reaction of Si in its electronic ground state with H_2 to form SiH + H is endothermic by about 35 kcal mol^{-1} (Zanchet et al. 2018) and therefore does not take place at the temperatures involved in our experiment (see below). However, to date, no data are available for the radiative association reaction $Si + H \rightarrow SiH$, nor for the bimolecular reaction of electronically excited Si with H_2 to form SiH + H, though $Si(^1D)$ has been shown to be highly reactive with, e.g., hydrocarbons (Yang et al. 2019). Our results from OES suggest that excited Si atoms are consumed in the reaction with H to form SiH and, therefore, in our case, since radiative association reactions are usually slow, the chemistry is initiated by the

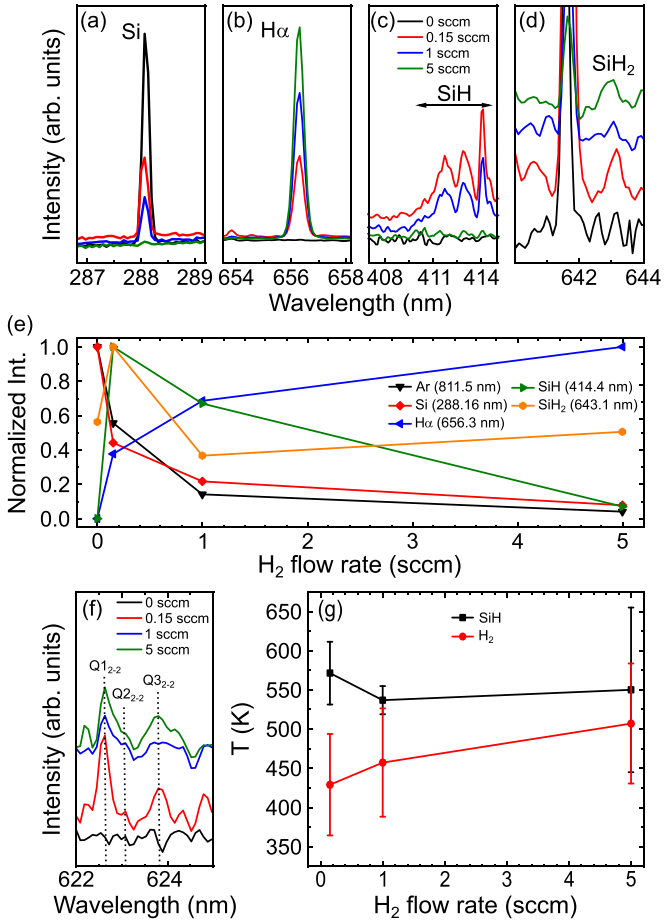

Figure 1. Optical emission spectra obtained during the experiment. The optical emission of Si (a), Hα (b), SiH (c), and SiH_2 (d) are displayed for increasing H_2 flow rate. In (d), the curves have been vertically shifted for clarity. (e) Evolution of the Ar, Si, Hα, SiH, and SiH_2 line intensities with the H_2 flow rate. The wavelength employed for each line is indicated in the figure. (f) Optical emission of the $Q1_{2-2}$, $Q2_{2-2}$, and $Q3_{2-2}$ rovibrational transitions of H_2 used to derive the gas temperature in the plasma. The curves have been vertically shifted for clarity. (g) Derived gas temperatures of SiH and H_2 at a distance of 1 cm from the magnetron target surface at the different H_2 flow rates used.

three-body reaction $Si + H + Ar \rightarrow SiH + Ar$, in which Ar (the sputtering gas) accelerates the chemistry. Moreover, the bimolecular reaction of electronically excited Si with H_2 to form SiH + H might contribute as well. Once SiH is formed, SiH_2 is produced through $SiH + H + Ar \rightarrow SiH_2 + Ar$, as suggested by the behavior of SiH and SiH_2 with respect to the H_2 flow rate (Figure 1(e)).

From the OES measurements, we have also derived the rotational temperatures of H_2 and SiH, which, in the case of equilibrium with the translational temperature, can be considered as the gas temperature in the plasma (Shimada et al. 2006). This condition is met in magnetron sputter sources since the pressure of the sputtering gas employed guarantees enough collisions for the rotational and translational temperatures to be in equilibrium (How et al. 2018). In the case of SiH we have simulated the emission spectra using the LIFBASE software (Luque & Crosley 1999) at several rotational temperatures, whereas in the case of H_2 we have obtained the rotational temperature by applying the Boltzmann plot method to the Q-branch ($\Delta J = 0$) rovibrational transitions $Q1_{2-2}$ ($\lambda = 622.58$ nm), $Q2_{2-2}$ ($\lambda = 623.06$ nm), and $Q3_{2-2}$ ($\lambda = 623.82$ nm) observed within

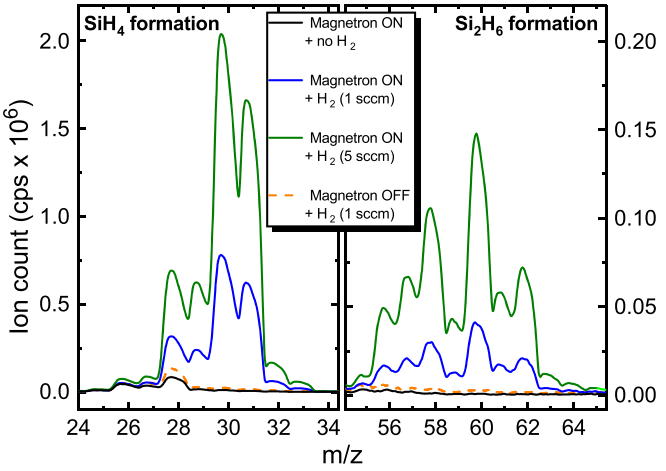

Figure 2. Mass spectra of the gas-phase products formed during the experiments. The increase of the peaks between $m/z = 28$ and $m/z = 33$ demonstrates silane (SiH_4) formation, whereas the increase of the peaks between $m/z = 56$ and $m/z = 62$ demonstrates disilane (Si_2H_6) formation.

the Fulcher-α ($d^3\Pi_u - a^3\Sigma_g^+$) band (Shikama et al. 2007) (Figure 1(f)). Rotational temperatures of around 550 K for SiH and 470 K for H_2 have been derived at all the H_2 flow rates employed (Figure 1(g)). These temperatures have been obtained from measurements at a distance of 1 cm from the target surface and, therefore, the gas temperature has already been decreased by collisions in the plasma expansion, implying that the gas temperature closer to the sputter target surface might be higher.

Figure 2 shows the mass spectrometry results. In the absence of H_2, only residual gas traces are detected, indicating that, within the sensitivity of the instrument, no gas-phase species are formed. Once H_2 is injected, we detect a number of peaks ranging from $m/z = 28$ to $m/z = 33$ and from $m/z = 56$ to $m/z = 62$, which correspond to the electron-impact dissociation patterns of silane (Kramida et al. 2020) and disilane (Simon et al. 1992), respectively. Moreover, Figure 2 shows that the amount of both molecules scales up with the H_2 flow rate. Hence, SiH and SiH_2 radicals, detected by OES once H_2 is injected into the chamber, are the primary products that further react with H and/or H_2 to give rise to SiH_4 and Si_2H_6. In our experimental conditions, the possible reactions leading to the formation of silane are:

$SiH + H \rightarrow SiH_2$ (Raghunath et al. 2013)
$SiH + H_2 \rightarrow SiH_3$ (Walch & Dateo 2001)
$SiH_2 + H \rightarrow SiH_3$ (Raghunath et al. 2013)
$SiH_3 + H \rightarrow SiH_4$ (Takahashi et al. 1994)
$SiH_2 + H_2 \rightarrow SiH_4$ (Adamczyk et al. 2010),

and to the formation of disilane:

$SiH_3 + SiH_3 \rightarrow Si_2H_6$ (Matsumoto et al. 1996)
$SiH_2 + SiH_4 \rightarrow Si_2H_6$ (Matsumoto et al. 2005),

which are summarized in Figure 3. All the radiative association reactions listed above are very slow and, therefore, in our case Ar acts as a third body accelerating the chemistry.

Apart from the gas-phase products, the interaction of silicon and hydrogen also produced solid dust analogs that consist of spherical nanoparticles, as shown in the AFM images of Figure 4. In the absence of H_2, Si atoms ejected from the magnetron aggregate and form solid nanoparticles (Figure 4(a)), although their formation rate is low. Injection of hydrogen into

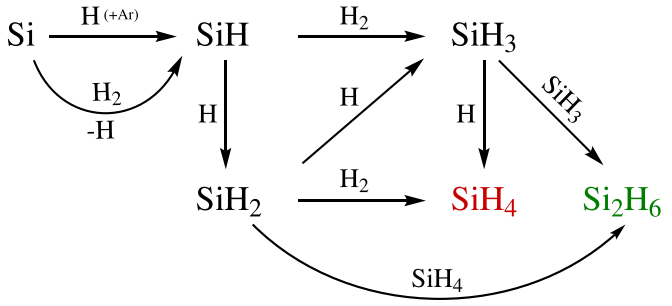

Figure 3. Scheme of the chemical reactions involved in the formation of SiH_4 and Si_2H_6. In our case the chemistry is initiated by the three-body reaction $Si + H + Ar \rightarrow SiH + Ar$. Moreover, the bimolecular reaction $Si + H_2 \rightarrow SiH + H$ with atomic Si in an electronically excited state might contribute as well. Subsequently, since radiative association reactions for these species are slow, in our experiments the growth of Si_nH_m species proceeds through three-body reactions with Ar (the sputtering gas).

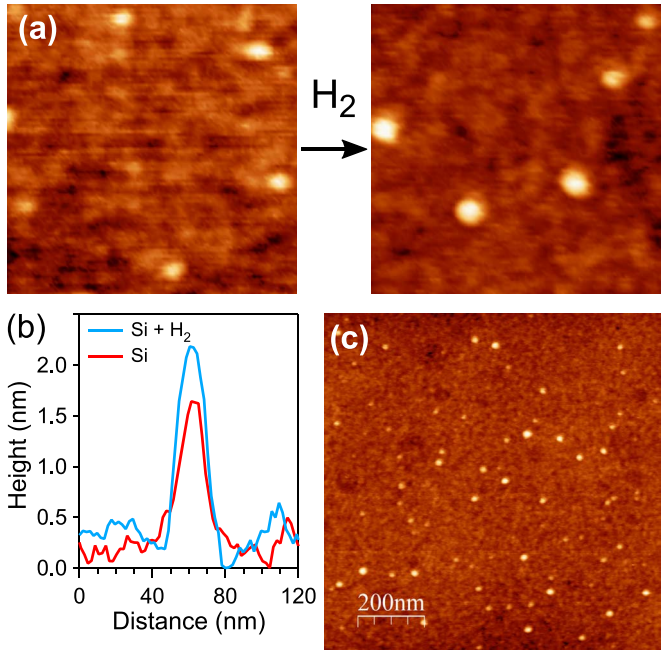

Figure 4. (a) AFM images (200 × 200 nm^2) of silicon nanoparticles: pure Si (left) and $Si + H_2$ (1 sccm) (right). (b) The height profiles of the nanoparticles show the increase in size after H_2 injection. (c) Lower magnification image of nanoparticles prepared following the reaction $Si + H_2$ (1 sccm).

the system boosts the particle size and production efficiency (Figure 4(c)). The particle formation rate increases by more than 30 times, as derived from substrate coverage measurements, and the average size of the grains increases upon the introduction of hydrogen into the system from 1.5 ± 0.2 nm (pure Si chemistry) to 2.1 ± 0.2 nm (H_2 injected in the chamber), extracted from statistical analysis of the AFM images. Figure 4(b) shows typical height profiles of the nanoparticles produced with and without hydrogen.

The solid dust analogs have also been characterized using three complementary characterization techniques: FTIR, XPS, and TPD. The infrared spectrum of the dust analogs shown in Figure 5(a) exhibits a band centered at 2125 cm^{-1} and a doublet (909 and 869 cm^{-1}) attributable, to SiH_x stretching and SiH_x bending/scissoring modes, respectively (Stryahilev et al. 2000). An FTIR spectrum of a fresh sample exposed to a controlled amount of water vapor (partial pressure equal to

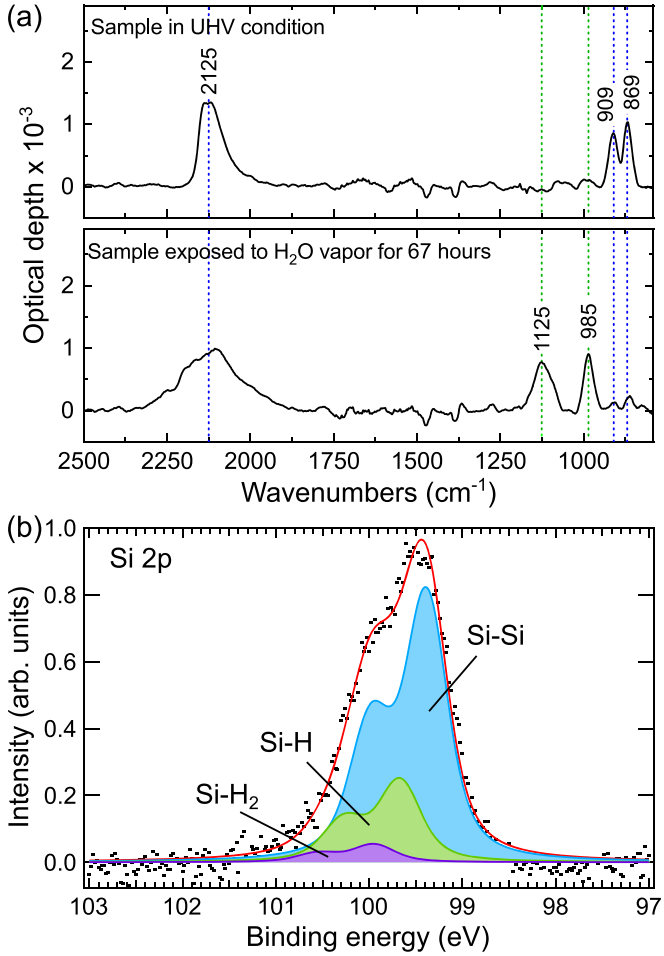

Figure 5. (a) FTIR spectra of the solid material synthesized following the $Si + H_2$ (1 sccm) reaction. Top panel: spectrum of the as-grown sample. Bottom panel: spectrum of the same sample after water vapor exposure for 67 hr. (b) High-resolution XPS scan for the Si 2p core level peak of the solid material synthesized following the $Si + H_2$ (1 sccm) reaction along with its deconvolution into components. Black dots: experimental data points. Red line: best fit.

1.0×10^{-6} mbar during 67 hr) is shown in the lower panel of Figure 5(a). The intensity of the SiH_x bending modes strongly decreases and two new features emerge at 1125 and 985 cm^{-1}, attributable to Si–O–Si stretching (Sabri et al. 2014) and to Si–OH bending (Carteret 2006) vibrations, respectively. Moreover, the shape and the intensity of the 2125 cm^{-1} band is modified after water vapor exposure; in particular, the broadening of this band toward higher wavenumbers is indicative of silicon oxidation (Moore et al. 1991).

In Figure 5(b), we present a high-resolution XPS spectrum of the Si 2p peak. Comparing this peak with the well-determined binding energy for Si 2p in the Si–Si configuration (99.5 eV), we can estimate the hydrogen content of the nanoparticles. Silicon oxide components, expected at 102–104 eV, are not present, indicating the absence of oxidation. The peak can be deconvolved into three doublet components, each doublet arising from spin–orbit splitting with $\Delta = 0.6$ eV (Lu et al. 1993). Each component is a signature of Si atoms in the nanograins with a distinct chemical/electronic environment. The Si $2p_{3/2}$ core level has three components whose maxima correspond to binding energies of 99.4, 99.7, and 100.0 eV (blue, green, and purple components in Figure 5(b) respectively), which can be readily assigned to Si–Si, Si–H, and

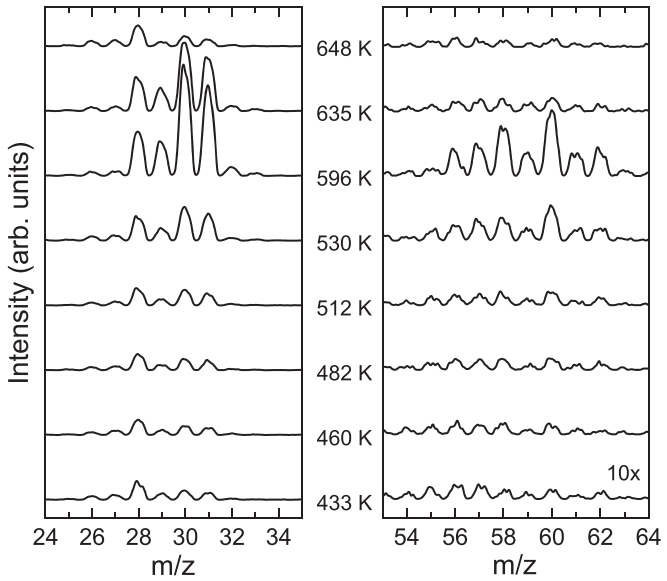

Figure 6. Thermal desorption of silane and disilane detected by the mass spectrometer during the annealing of the solid material synthesized following the Si + H_2 (1 sccm) reaction. The curves have been vertically shifted and the signal from $m/z = 53$ to $m/z = 64$ has been magnified 10 times for the sake of clarity.

Si–H_2 species, respectively (Cerofolini et al. 2003). From the relative intensities of the components, we can estimate the relative abundance of Si atoms in every bonding configuration. The intensity analysis yields 73% in Si–Si, 23% in Si–H, and 5% in Si–H_2.

Finally, we have characterized the dust grains by means of TPD. Figure 6 shows clear desorption of silane ($m/z = 28$–33) and disilane ($m/z = 56$–62) from the solid-state material within the temperature range 530–648 K, being the intensity of disilane about 15 times lower than that of silane.

All the experimental results suggest that the dust analogs are composed of amorphous hydrogenated silicon (a-Si:H) (Street 1991). This material consists of a random network of Si atoms in sp^3 hybridization and covalently bonded to four immediate neighbors, which can be either Si or H atoms exclusively. Amorphous hydrogenated silicon can be grown in thin films by magnetron sputtering of Si targets in the presence of hydrogen (Langford et al. 1992) with a final hydrogen content ranging between 8% and 45% (Street 1991). In addition, annealing of a-Si:H is known to produce major structural changes in the material, with massive outgassing starting above 625 K, corresponding to conversion of SiH_3 groups to SiH_2 and SiH (Langford et al. 1992). In our case, a-Si:H is grown in grains with a hydrogen content of about 15% as derived from XPS measurements. As the material is heated during the TPD experiments, the highly reactive silicon–hydrogen species produced during the thermal processing of the grains react with trapped H_2 and between them to form the more stable saturated molecules silane and disilane. Note that the IR spectrum of Figure 5(a) contains the same bands as those of a-Si:H (Langford et al. 1992).

4. Discussion

Our experiments evidence that atomic SiH, and H_2 efficiently react in the gas phase to form silane, disilane, and amorphous hydrogenated silicon nanoparticles. As monitored by OES, the synthesis of the two gaseous species is mediated by the formation of SiH and SiH_2. The former is produced by the three-body reaction $Si + H + Ar \rightarrow SiH + Ar$, which involves the sputtering gas, and the bimolecular reaction of electronically excited Si with H_2 to form SiH + H might contribute as well. Once SiH is produced, SiH_2 forms in our case from the reaction of SiH and H with Ar as a third body, since radiative association reactions are slow for these species. Subsequently, SiH and SiH_2 can react with atomic and molecular hydrogen to form the saturated Si compounds (Si_nH_{2n+2}) through three-body reactions in which Ar acts as a third body accelerating the chemistry.

From the astrochemical perspective, silicon and hydrogen have high cosmic abundances, and thus silane and silane derivatives are candidates to be present in interstellar and circumstellar environments. To date, silane has been firmly detected only in the CSE of the carbon-rich AGB star IRC +10216 (Goldhaber & Betz 1984), whereas disilane has never been detected in space. The importance of silane chemistry in the CSE of IRC+10216 is stressed by the detection of methyl silane and silyl cyanide by Cernicharo et al. (2017). However, the radius at which silane is formed in IRC +10216 is not well constrained. Keady & Ridgway (1993) suggest that it could be formed at 40 stellar radii based on the analysis of the profiles of several rovibrational lines, which set an upper temperature limit of about 280 K for silane formation, whereas Monnier et al. (2000) claim that the formation of silane occurs at ~80 stellar radii, based on interferometric observations of one of its rovibrational lines. The derived abundance of silane (around 2×10^{-7} relative to H_2) is larger than predicted by thermochemical equilibrium by several orders of magnitude (Gail & Sedlmayr 2013; Agúndez et al. 2020), and thus it has been suggested that SiH_4 could be formed by catalytic reactions at the surface of dust grains (Keady & Ridgway 1993; Monnier et al. 2000). On the other hand, chemical calculations including the effect of shock waves in the inner region of IRC+10216 predict that SiH_4 can be formed at 5 stellar radii, although at low abundances (Willacy & Cherchneff 1998)

Our results present a mechanism to form silane from atomic silicon and molecular hydrogen in the innermost regions of the CSEs of C-rich AGB stars like IRC +10216. Thermochemical equilibrium predicts that atomic silicon is very abundant in the inner regions (up to ~5 stellar radii) of carbon-rich envelopes, although at larger distances SiS, SiO, and silicon carbides are predicted to trap most of the silicon (Gail & Sedlmayr 2013; Agúndez et al. 2020). Nevertheless, there are evidences of nonthermal equilibrium in the in the inner wind of AGB stars, for instance the ascertained presence of a few molecules not expected to form under thermal equilibrium (Agúndez et al. 2020). Thus, models based on nonequilibrium chemistry predict that atomic silicon can be injected into carbon-rich expanding envelopes with fairly large abundances (Cherchneff 2006), and its abundance, for carbon stars, increases with radius. Moreover, other refractory elements, such as Na, K, Ca, Cr, and Fe, have been observed to be present in atomic form in the outer envelope of IRC +10216 (Mauron & Huggins 2010). However, our experiments indicate that three-body reactions are needed to form SiH_x ($x = 1$–4) species from atomic Si and atomic and molecular hydrogen at sufficient reaction rates and, thus, the gas-phase synthesis of SiH_4 is only possible at distances lower than 10 stellar radii, even if atomic Si is present in the outer envelope. Our results also point toward the gas-phase synthesis of disilane in the inner envelope, and the work

of Kaiser & Osamura (2005) could guide the search for Si_2H_x species through infrared observations.

As mentioned above, the formation of SiH_4 in IRC+10216 is thought to start at 40 stellar radii, suggesting that the main contribution to the formation of silane might come from chemical reactions catalyzed on the surface of dust grains (Keady & Ridgway 1993) with the condensation of Si-bearing molecules on the grains and surface diffusion of those playing a major role (Monnier et al. 2000). These are likely the main mechanisms of SiH_4 formation in IRC+10216 since, if gas-phase synthesis were the main mechanism, the abundance of SiH_4 would follow a different spatial distribution. Nevertheless, based on our results, a contribution from gas-phase synthesis, even if small, might start earlier in the expanding wind of IRC +10216. The fact that SiH_4 is not detected at distances lower than 40 R_* indicates that the gas-phase reactions might be slow and with lower reaction rates than other competing reactions of atomic Si with, e.g., C_2H_2.

In addition to the products formed in the gas phase, in our experiments we have generated amorphous hydrogenated silicon grains, which consist of a random three-dimensional network in which silicon atoms are tetragonally bonded to other silicon and hydrogen atoms. In fact, both XPS and FTIR spectroscopy indicate that hydrogen atoms are bound to the silicon atoms. TPD experiments show that these nanograins decompose at temperatures above 530 K, leading to silane and disilane. To date, there is not observational evidence of the presence of solid hydrogenated silicon in space. Whether this kind of grain is present in interstellar and circumstellar media is still unclear and the fact that this material is more thermally unstable than other Si-containing condensates plays against its presence in space, since the formation of dust in envelopes around AGB stars takes place as the expanding gas cools down to temperatures below 1500–1000 K. In this temperature range, Si-containing solids like SiC (in the case of C-rich envelopes) and silicates (in O-rich environments) condense. Therefore, it is likely that at lower temperatures, where a-Si:H can form without thermally decomposing, most silicon has been already locked by more refractory condensates. However, we note that since dust formation in AGB star ejecta occurs out of equilibrium (Gail & Sedlmayr 2013), the way in which silicon condenses does not need to strictly follow the condensation sequence given by a thermochemical equilibrium. For instance, condensates like MgS, which have fairly low condensation temperatures (<600 K; Lodders & Fegley 1999; Agúndez et al. 2020), have been proposed to be part of the dust grain composition in carbon-rich AGB stars (Goebel & Moseley 1985). Thus, if hydrogenated silicon grains form in carbon-rich CSEs, processing by ultraviolet photons and/or cosmic rays penetrating into intermediate layers of the envelope might lead to the formation of silane. This is not likely to be the main mechanism for silane formation, but it could contribute to justify its amount, 6 times higher than the one predicted by models based on thermodynamic equilibrium.

Finally, our experiments have also shown the conversion of Si–H bonds to Si–O–Si and Si–OH bonds upon exposure of the hydrogenated silicon nanoparticles to water vapor. Si–H bonds are known to exhibit a high reactivity with oxygen-bearing species (Nuth et al. 1992). If hydrogenated silicon is present in the interstellar medium, in the colder regions where dust grains are coated by icy species, mainly H_2O, it is likely that it is oxidized, forming silicates.

5. Conclusions

The experimental results presented here provide a possible and efficient mechanism for the formation of silane and disilane in the gas phase from Si, H, and H_2 in the innermost regions of the CSEs around AGB stars. Most likely, the main formation mechanism of SiH_4 in C-rich stars, as suggested by observations, involves the catalysis on the surface of dust grains since gas-phase reactions are only efficient in the inner parts of the envelope and cannot explain the observed abundances of silane and its derivatives in the CSE of IRC+10216. In our experiments, hydrogenated silicon dust (a-Si:H) particles are also formed, the thermal processing of which produces SiH_4 and Si_2H_6 at temperatures above 530 K. This kind of grain could form and survive without thermally decomposing in regions of AGB envelopes where temperatures are below ~500 K and, if exposed to energetic photons or particles, could become a source of silane. In addition, we have observed that the exposure of the a-Si:H dust particles to water vapor promotes the formation of SiO and SiOH groups at the expense of SiH moieties. Therefore, if hydrogenated silicon dust is coated with water ices in the interstellar medium, it will most likely turn into silicate grains.

We thank the European Research Council for funding support under Synergy grant ERC-2013-SyG, G.A. 610256 (NANOCOSMOS). Also, we acknowledge partial support from the Spanish MINECO through grants MAT2017-85089-c2-1R, FIS2016-77726-C3-1-P, FIS2016-77578-R, AYA2016-75066-C2-1-P and RyC-2014-16277. Support from the FotoArt-CM Project (P2018/NMT 4367) through the Program of R&D activities between research groups in Technologies 2013, cofinanced by European Structural Funds, is also acknowledged. G.T.C. acknowledges funding from the Comunidad Autónoma de Madrid (PEJD-2018-PRE/IND-9029).

ORCID iDs

Mario Accolla https://orcid.org/0000-0002-9509-5967
Gonzalo Santoro https://orcid.org/0000-0003-4751-2209
Pablo Merino https://orcid.org/0000-0002-0267-4020
Lidia Martínez https://orcid.org/0000-0002-9370-2962
Guillermo Tajuelo-Castilla https://orcid.org/0000-0001-7877-2543
Luis Vázquez https://orcid.org/0000-0001-6220-2810
Jesús M. Sobrado https://orcid.org/0000-0002-7359-0262
Marcelino Agúndez https://orcid.org/0000-0003-3248-3564
Miguel Jiménez-Redondo https://orcid.org/0000-0001-9221-8426
Víctor J. Herrero https://orcid.org/0000-0002-7456-4832
Isabel Tanarro https://orcid.org/0000-0002-1888-513X
José Cernicharo https://orcid.org/0000-0002-3518-2524
José Ángel Martín-Gago https://orcid.org/0000-0003-2663-491X

References

Adamczyk, A. J., Reyniers, M.-F., Marin, G. B., & Broadbelt, L. J. 2010, PCCP, 12, 12676
Agúndez, M., Cernicharo, J., & Guélin, M. 2014, A&A, 570, A45
Agúndez, M., Martínez, J. I., de Andres, P. L., Cernicharo, J., & Martín-Gago, J. A. 2020, A&A, 637, A59
Apponi, A. J., McCarthy, M. C., Gottlieb, C. A., & Thaddeus, P. 1999, ApJL, 516, L103
Carteret, C. 2006, AcSpA, 64, 670

Cernicharo, J., Agúndez, M., Velilla Prieto, L., et al. 2017, A&A, 606, L5
Cernicharo, J., Gottlieb, C. A., Guelin, M., Thaddeus, P., & Vrtilek, J. M. 1989, ApJL, 341, L25
Cernicharo, J., McCarthy, M. C., Gottlieb, C. A., et al. 2015, ApJL, 806, L3
Cerofolini, G. F., Galati, C., & Renna, L. 2003, SurIA, 35, 968
Cherchneff, I. 2006, A&A, 456, 1001
Escribano, R., & Campargue, A. 1998, JChPh, 108, 6249
Fogerty, S., Forrest, W., Watson, D. M., Sargent, B. A., & Koch, I. 2016, ApJ, 830, 71
Gail, H.-P., & Sedlmayr, E. 2013, Physics and Chemistry of Circumstellar Dust Shells (Cambridge: Cambridge Univ. Press) doi:10.1017/CBO9780511985607
Goebel, J. H., & Moseley, S. H. 1985, ApJL, 290, L35
Goldhaber, D. M., & Betz, A. L. 1984, ApJL, 279, L55
Guélin, M., Muller, S., Cernicharo, J., et al. 2000, A&A, 363, L9
Guélin, M., Muller, S., Cernicharo, J., McCarthy, M. C., & Thaddeus, P. 2004, A&A, 426, L49
Hanfland, M., Proctor, J. E., Guillaume, C. L., Degtyareva, O., & Gregoryanz, E. 2011, PhRvL, 106, 095503
Henning, T. 2010, ARA&A, 48, 21
Horcas, I., Fernández, R., Gómez-Rodríguez, J. M., et al. 2007, RScI, 78, 013705
How, S. R., Nayan, N., Lias, J., et al. 2018, JPhCS, 1027, 012005
Kaiser, R. I., & Osamura, Y. 2005, A&A, 432, 559
Keady, J. J., & Ridgway, S. T. 1993, ApJ, 406, 199
Kramida, A., Ralchenko, Y., & Reader, J. 2020, NIST Atomic Spectra Database (v5.8)
Langford, A. A., Fleet, M. L., Nelson, B. P., Lanford, W. A., & Maley, N. 1992, PhRvB, 45, 13367
Lodders, K., & Fegley, B. 1999, in IAU Symp. 191, Asymptotic Giant Branch Stars, ed. T. Le Bertre, A. Lebre, & C. Waelkens (Cambridge: Cambridge Univ. Press), 279
Lu, Z. H., Graham, M. J., Jiang, D. T., & Tan, K. H. 1993, ApPhL, 63, 2941
Luque, J., & Crosley, D. 1999, SRI Interantional Report MP 99-009, https://archive.sri.com/engage/products-solutions/lifbase
Martínez, L., Lauwaet, K., Santoro, G., et al. 2018, NatSR, 8, 7250
Martínez, L., Santoro, G., Merino, P., et al. 2020, NatAs, 4, 97
Massalkhi, S., Agúndez, M., Cernicharo, J., et al. 2018, A&A, 611, A29
Matsumoto, K., Klippenstein, S. J., Tonokura, K., & Koshi, M. 2005, JPCA, 109, 4911
Matsumoto, K., Koshi, M., Okawa, K., & Matsui, H. 1996, JPhCh, 100, 8796
Mauron, N., & Huggins, P. J. 2010, A&A, 513, A31
McCarthy, M. C., Gottlieb, C. A., & Thaddeus, P. 2003, MolPh, 101, 697
Monnier, J. D., Danchi, W. C., Hale, D. S., Tuthill, P. G., & Townes, C. H. 2000, ApJ, 543, 868
Moore, M. H., Tanabe, T., & Nuth, J. A. 1991, ApJL, 373, L31
Nuth, J. A., III, Moore, M. H., Tanabe, T., & Kraus, G. 1992, Icar, 98, 207
Ohishi, M., Kaifu, N., Kawaguchi, K., et al. 1989, ApJL, 345, L83
Perrin, J., & Delafosse, E. 1980, JPhD, 13, 759
Raghunath, P., Lee, Y.-M., Wu, S.-Y., Wu, J.-S., & Lin, M.-C. 2013, IJQC, 113, 1735
Sabri, T., Gavilan, L., Jäger, C., et al. 2014, ApJ, 780, 180
Santoro, G., Martínez, L., Lauwaet, K., et al. 2020a, ApJ, 895, 97
Santoro, G., Sobrado, J. M., Tajuelo-Castilla, G., et al. 2020b, RScI, 91, 124101
Shikama, T., Kado, S., Zushi, H., & Tanaka, S. 2007, PhPl, 14, 072509
Shimada, M., Tynan, G. R., & Cattolica, R. 2006, JVSTA, 24, 1878
Simon, J., Feurer, R., Reynes, A., & Morancho, R. 1992, J. Anal. Appl. Pyrolysis, 24, 51
Street, R. A. 1991, Hydrogenated Amorphous Silicon (Cambridge: Cambridge Univ. Press)
Striganov, A. R., & Sventitskii, N. S. 1968, Tables of Spectral Lines of Neutral and Ionized Atoms (New York: Springer US),
Stryahilev, D., Diehl, F., & Schröder, B. 2000, JNCS, 266–269, 166
Takahashi, J., Momose, T., & Shida, T. 1994, Bull. Chem. Soc. Japan, 67, 74
Thaddeus, P., Cummins, S. E., & Linke, R. A. 1984, ApJL, 283, L45
Tiemann, E., Renwanz, E., Hoeft, J., & Törring, T. 1972, ZNatA, 27, 1566
Törring, T. 1968, ZNatA, 23, 777
Treffers, R., & Cohen, M. 1974, ApJ, 188, 545
Turner, B. E. 1992, ApJL, 388, L35
Walch, S. P., & Dateo, C. E. 2001, JPCA, 105, 2015
Waters, L. B. F. M., Molster, F. J., de Jong, T., et al. 1996, A&A, 315, L361
Willacy, K., & Cherchneff, I. 1998, A&A, 330, 676
Wyller, G. M., Preston, T. J., Klette, H., et al. 2016, Energy Proc., 92, 904
Yang, T., Bertels, L., Dangi, B. B., et al. 2019, PNAS, 116, 14471
Yang, T., Dangi, B. B., Maksyutenko, P., et al. 2015, JPCA, 119, 12562
Zanchet, A., Roncero, O., Agúndez, M., & Cernicharo, J. 2018, ApJ, 862, 38